Carbohydrate Polymers 92 (2013) 2232–2238

Contents lists available at SciVerse ScienceDirect

Carbohydrate Polymers

journal homepage: www.elsevier.com/locate/carbpol

Poly(vinyl alcohol)/sodium alginate/layered silicate based nanofibrous mats for bacterial inhibition

Wei Li[a,b,1], Xueyong Li[c,1], Yang Chen[d], Xiaoxia Li[e], Hongbing Deng[a,b,*], Ting Wang[b], Rong Huang[b], Gang Fan[b]

[a] School of Resource and Environmental Science, Wuhan University, Wuhan 430079, China
[b] College of Food Science and Technology, Huazhong Agricultural University, Wuhan 430070, China
[c] Department of Plastic Surgery, Tangdu Hospital, Fourth Military Medical University, Xi'an 710032, China
[d] Zhongnan Hospital, Wuhan University, Wuhan 430071, China
[e] School of Chemistry and Chemical Engineering, Wuhan Textile University, Wuhan 430073, China

ARTICLE INFO

Article history:
Received 26 June 2012
Received in revised form
23 September 2012
Accepted 3 December 2012
Available online 12 December 2012

Keywords:
Electrospinning
Poly(vinyl alcohol)
Alginate
Organic rectorite
Bacterial inhibition activity

ABSTRACT

Poly(vinyl alcohol) (PVA)/sodium alginate (ALG)/organic rectorite (OREC) composite nanofibrous mats are fabricated by electrospinning aqueous solutions with different mixing ratios. Both good fiber shape and three-dimensional structure of nanofibrous mats can be observed by Field Emission Scanning Electron Microscopy. Energy-dispersive X-ray spectroscopy shows the existence of OREC in the as-spun composite mats. In addition, small-angle X-ray diffraction confirms that the interlayer of OREC is intercalated by ALG/PVA chains, and the distance between OREC interlayers is increased from 4.50 to 4.74 nm. Wide angle X-ray diffraction and Fourier transform infrared spectra further verify the intercalation is between polymers and layered silicate. Moreover, the thermal gravimetric analysis shows that the addition of OREC has only a small effect on the thermal stability of composites. Furthermore, the antibacterial experiments illustrate that OREC can enhance the bacterial inhibition ability of nanofibrous mats against *Escherichia coli* and *Staphylococcus aureus*.

1. Introduction

Nanofibrous mats with bacterial inhibition activity have become more and more popular in the field of human health protection (Chen et al., 2011), and there are many processes for fabricating nanofibers, such as drawing, phase separation, self assembly, template synthesis and electrospinning (Wang, Ding, Yu, & Wang, 2011). Among these methods, electrospinning can be regard as the most effective and useful technique for producing continuous and uniform nanofibers with diameters between micrometers and nanometers via electrostatically driven jets of polymer solution or melts. Besides, ultra fine diameters (Deng et al., 2010), high surface area to volume (Mimura et al., 2011) and three-dimensional (3D) structure (Ding, Kim, Kimura, & Shiratori, 2004) are also important properties of electrospun nanofibers. At present, the electrospun nanofibrous mats have been applied in wound healing (Noh et al., 2006), sensors (Mimura et al., 2011), tissue engineering (Deng et al., 2010), drug delivery (Hou et al., 2011) and antibacterial applications (Deng, Li, & et al., 2011; Deng et al., 2012).

Compared with the pure polymer, polymer/layered silicate composites combine the physical and chemical properties of both inorganic and organic materials (Wang, Du, Yang, Tang, & Luo, 2008; Wang et al., 2009; Deng et al., 2012) in order to enhance properties such as surface area to volume ratio, thermal stability, antibacterial activity and drug controlled release ability. Indeed, recent studies (Wang et al., 2006, 2008; Deng, Li, & et al., 2011; Deng et al., 2012) have shown that the antibacterial activity can be enhanced with the addition of organic rectorite (OREC). Interestingly, the European Food Safety Authority (EFSA) have recently reported the safety of layered silicate particularly bentonite (dioctahedral montmorillonite) and verified that bentonite as food additives was safe to reduce milk aflatoxin by adsorption (EFSA, 2011). Non-toxic, biocompatible and biodegradable natural polymers, such as chitosan and alginate, have been applied as bacteriostatic agents. In fact, sodium alginate (ALG) has become more and more widely used in food preservation and wound healing. Considering the above merits, ALG and OREC are selected as the candidates for bacterial inhibition.

OREC, a kind of layered silicate modified from rectorite (REC), has a larger interlayer distance, better separable layer thickness and

* Corresponding author at: Wuhan University, School of Resource and Environmental Science, Wuhan 430079, China. Tel.: +86 27 68778501; fax: +86 27 68778501.
E-mail address: alphabeita3000@yahoo.com.cn (H. Deng).
[1] Co-first author with the same contribution to this work.

0144-8617/$ – see front matter © 2012 Elsevier Ltd. All rights reserved.
http://dx.doi.org/10.1016/j.carbpol.2012.12.004

layer aspect ratio than REC and montmorillonite (Wang et al., 2006; Dang, Wang, & et al., 2011; Deng et al., 2012). As a inorganic substance, OREC also exhibits the same properties as typical inorganic materials, such as long life expectancy, high heat resistance and weak mould proof activity (Guo, Ma, Guo, & Xu, 2005), which also has potential applications in various fields such as drug delivery (Guo et al., 2005; Wang et al., 2008) and antibacterial applications (Deng, Li, & et al., 2011; Deng, Wang, & et al., 2011; Deng et al., 2012).

ALG is an anionic polysaccharide contained β-D-mannuronate (M) and α-L-guluronate (G) residues in the natural. ALG can be blended compatibility with organic matrixes (Suci, Vrany, & Mittelman, 1998). The attempt to further make use of the hydrogel properties and biocompatibility in ALG has shown enhanced performance in drug delivery (Xu et al., 2013), wound healing (Balakrishnan, Mohanty, Umashankar, & Jayakrishnan, 2005) and et al. In addition, some literature (Walker, Hobot, Newman, & Bowler, 2003; Covarrubias, de-Bashan, Moreno, & Bashan, 2012) reports that bacteria tend to be immobilized onto ALG so ALG may be a potential antibacterial agent.

Unfortunately, due to the lack of chain entanglements caused by the rigid and extended chain conformation in aqueous solution (Islam & Karim, 2010), ALG is difficult to be directly fabricated into nanofibrous mats, and the electrospinning of ALG is still challenging. Due to its excellent biocompatibility and good spinnability, PVA is an ideal candidate for improving the electrospinnability of ALG based solutions. PVA nanofibers have high tensile, strength, tensile modulus and abrasion resistance (Lee et al., 2004).

According to our previously reports (Deng, Li, & et al., 2011; Deng, Wang, & et al., 2011; Deng et al., 2012), the positively charged chitosan can be intercalated into the interlayer of OREC. Therefore, we suppose that the chains of negatively charged ALG can also enter into the interlayer of OREC to form composites with an intercalated structure. In this study, PVA/ALG/OREC composite nanofibrous mats with intercalated structure are fabricated via electrospinning. The properties and structure of nanofibrous mats were characterized. These include morphology, surface elements, thermal properties, crystalline structure and rheology. Finally, the bacterial inhibition assay will be used to investigate the antibacterial activity of composite fibrous mats.

2. Experimental details

Poly(vinyl alcohol) (PVA, $M_w = 9 \times 10^4$) were provided by Sigma Aldrich Chemical Reagent Co., USA. Calcium rectorite (Ca^{2+}-REC) was purchased from Hubei Mingliu Co., China. While sodium dodecylsulphonate (SDS), sodium alginate (ALG, $M_w = 2.5 \times 10^5$) and acetic acid were also supplied by Aladdin Chemical Reagent Co., Shanghai, China. Other chemicals of analytical grade were used as received without any further purification. All aqueous solutions were prepared using purified water with a resistance of 18.2 MΩ.cm.

10% PVA solution was prepared by dissolving PVA into purified water at 60 °C bath with gentle magnetic stirring for 4 h. 2% ALG solution was prepared by adding ALG powder into purified water with constant agitation in close vials for 5 h at room temperature. Organic rectorite (OREC) was prepared by SDS cation exchange reactions as described previously (Deng, Li, & et al., 2011; Deng, Wang, & et al., 2011; Deng et al., 2012). Briefly, the REC was dispersed into purified water with high-speed stirring for 24 h and then SDS added dropwise. The cation exchange reaction between SDS and REC could happen at 90 °C with 5 h gentle stirring. Finally, the products were freeze-dried and ground into a fine powder with a mortar.

PVA/ALG mixed solutions were obtained by mixing 10% PVA and 2% ALG together to achieve PVA/ALG mixture at 90/10, 80/20, 60/40 and 40/60 mass ratios, respectively. After ultrasonication, 1% OREC is added into each as-prepared PVA/ALG solution to get PVA/ALG/OREC solution. Finally, the mixtures were kept stirring for 48 h at room temperature. The concentrations of all above solutions were expressed in wt/wt%.

The as-prepared PVA/ALG and PVA/ALG/OREC solutions were loaded into a syringe equipped with a blunt needle with an internal diameter of needle was 0.8 mm. The constant flow rates ranging from 1 mL/h were modulated using by a syringe pump (LSP02-1B, Baoding Longer Precision Pump Co., Ltd., China). The tip-to-collector distance was 15 cm with the applied voltage of 15 kV by a high voltage power supply (DW-P303-1ACD8, Tianjin Dongwen High Voltage Co., China). The as-spun fibers were collected by a grounded collector covered with aluminum foil. The ambient temperature and relative humidity were kept at 25 °C and 45%, respectively. The prepared samples were dried in vacuum at room temperature for 24 h to remove the trace solvent.

The conductivity of the electrospinning solutions was determined by Mettler-Toledo Conductivity Meter (FE30, Switzerland). All the fibrous mats were processed by vacuum spray carbon before the conduction of the Field Emission Scanning Electron Microscopy (FE-SEM) images and energy-dispersive X-ray (EDX) spectroscopy (S-4800, FEI Ltd., Japan). Fourier transform infrared (FT-IR) spectra were identified by Nicolet170-SX (Thermo Nicolet Ltd., USA) in the wavenumber range of 4000–400 cm^{-1} and the number of FT-IR scans was 32 times. The X-ray diffraction (SAXRD) was carried out using a diffractrometer type D/max-rA (Rigaku Co., Japan) with Cu target and Ka radiation ($\lambda = 0.154$ nm). The scanning rate for the small-angle X-ray diffraction (SAXRD) was 1°/min and the scanning scope of 2θ was 1–6°. For the wide angle X-ray diffraction (WAXRD) the scanning rate was 1°/min and the scanning scope of 2θ was between 5 and 60°. Thermogravimetric analysis (TGA) was performed on Pyris 1 TGA at a heating rate of 20 °C/min from room temperature to 500 °C under a flow of air. The rheological properties of the composite solutions were measured with a Bohlin VOR strain-controlled solution rheometer at 25 °C using concentric cylinder geometry. Shear measurements were in a range of shear rates from 80 to 1000 s^{-1}.

The bacterial inhibition activity of the nanofibrous mats was measured according to the previous literatures (Li, Li, Ke, Shi, & Du, 2011; Deng et al., 2012). Disk-diffusion test was conducted to investigate the inhibitory effect of the mats. Gram-negative bacteria *Escherichia coli* (*E. coli*) and Gram-positive bacteria *Staphylococcus aureus* (*S. aureus*) were selected as the representative bacteria. The nanofibrous mats together with aluminum foil were cut into disks (diameter = 7 mm) and then sterilized with an ultraviolet radiation lamp for 30 min. 50 μL diluted levitation bacterial with a concentration of 5.0–10.0 × 10^5 cfu/mL were inoculated into the agar culture medium uniformly. After that, the disks were placed on the surface of the agar medium at 37 °C for 24 h. The inhibition zones were measured with a tolerance of 1 mm. Each sample was repeated three times.

3. Results and discussion

3.1. The morphology and EDX analysis of nanofibrous mats

The morphology of nanofibrous mats can be controlled by various parameters included applied voltage, distance between the needle tip and collector, solution feed rate and other solution parameters such as polymer concentration, polymer molecular weight and surface tension (Islam & Karim, 2010). The diameter and morphology of fibers changed remarkably when the

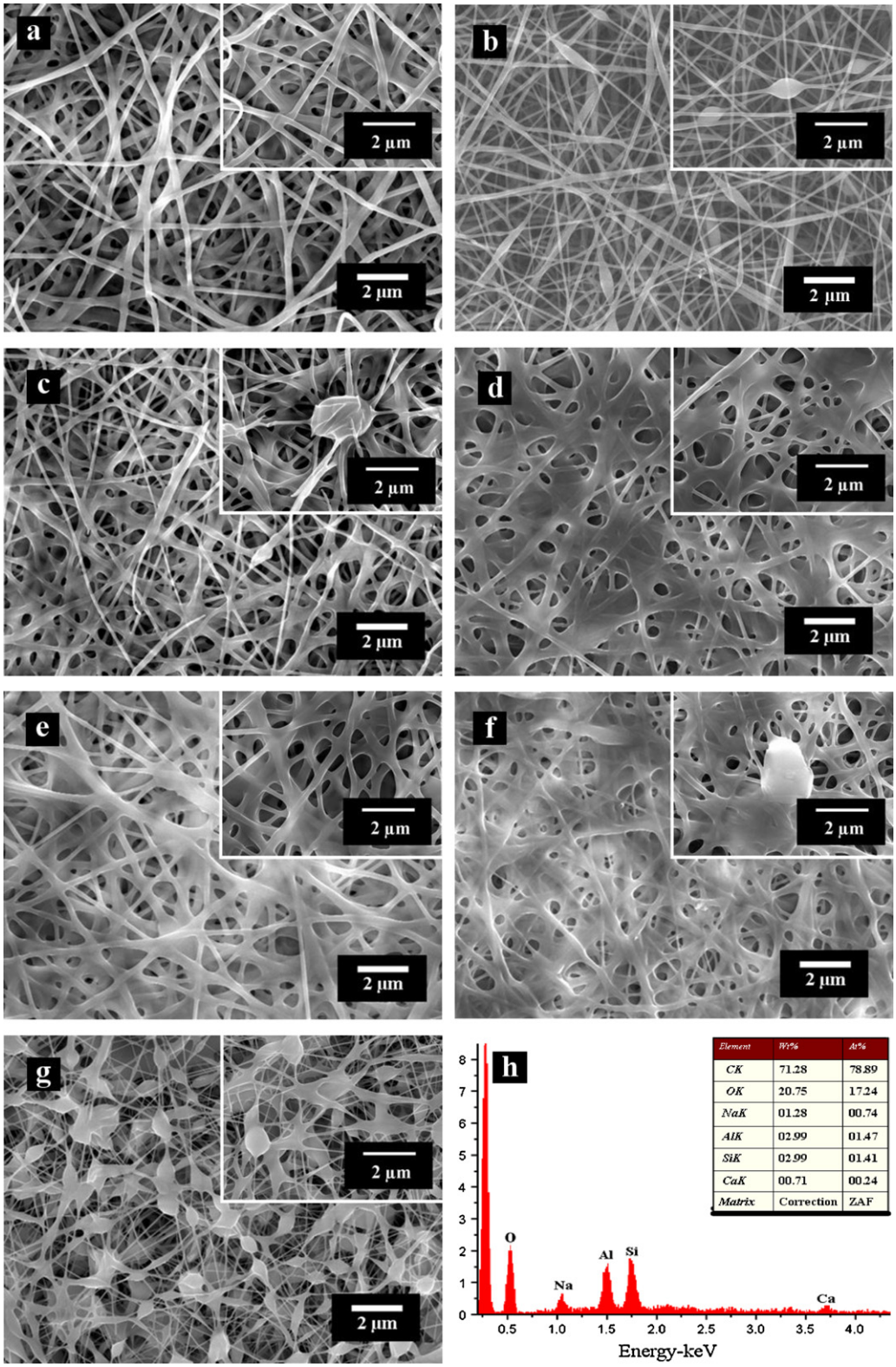

Fig. 1. FE-SEM images of nanofibrous mats electrospun from PVA/ALG solutions at different mass ratios (a) 100/0 and (b) 60/40, and nanofibrous mats electrospun from PVA/ALG solutions at different mass ratios containing 1% OREC: (c) 100/0, (d) 90/10, (e) 80/20, (f) 60/40 and (g) 40/60. (h) EDX spectroscopy of selected area from sample f.

component varied (Fig. 1a–g). With the outstanding film-forming and spinnability properties of PVA, the bulk PVA mats (Fig. 1a) with uniform nanofiber shape and 3D structure is extraordinary stabilized and continuous. Among the PVA/ALG (60/40) nanofibrous mats (Fig. 1b), a few spindle-like beads are observed (Islam & Karim, 2010).

Fig. 1c–g show the morphology of nanofibrous mats with different mass ratio of PVA/ALG containing 1% OREC. When the amount of ALG is increased, some junctions among the fibers lead the fibers to adhere with each other (Fig. 1c–f). This is caused by trace residual solvent after electrospinning. The main reason for this is that the water binding capacity of ALG and PVA is different. In fact,

Table 1
Conductivity of the composite PVA/ALG solutions at different mass ratios with constant content of 1% OREC.

Samples	Conductivity (μm/cm)
PVA	865
ALG	4090
PVA/ALG = 60/40	1634
PVA/OREC	670
(PVA/ALG = 90/10)/OREC	879
(PVA/ALG = 80/20)/OREC	1154
(PVA/ALG = 60/40)/OREC	1573
(PVA/ALG = 40/60)/OREC	2110

ALG has a high water binding capacity (Lee, Jeong, Kang, Lee, & Park, 2009), which is beneficial for the absorption of water around the fibers and the formation of fibers is also good. When PVA/ALG is 40/60, more beads connected with ultrathin fibers are formed (Fig. 1g). Compared Fig. 1a with c, as well as Fig. 1b with f, the result reveals that OREC can obviously affect the morphology of the as-spun nanofibrous mats.

To detect the surface compositions of composite nanofibrous mats, Energy-dispersive X-ray spectroscopy (Fig. 1h) was used. The characteristic chemical elements of OREC are Ca, Si and Al. In the EDX spectroscopy of PVA/ALG/OREC composite nanofibrous mats, the characteristic peaks of Ca, Si and Al are easily observed which verifies that OREC is successful incorporated into the composite nanofibrous mats. Besides, the characteristic peak of Na reveals that SDS or ALG is also existed in the composite nanofibrous mats.

3.2. Conductivity and rheology of the composite solutions

As shown in Table 1, the conductivity of ALG is the largest while that of PVA is the lowest. Obviously, the conductivity of bulk PVA is remarkably increased after blending with ALG, but it will reduce when 1% OREC is added. As expected, the addition of OREC has slightly affected the conductivity of solutions because OREC is positive charged (Wang et al., 2009). Compared with other solutions, ALG is considered as the greatest contributor to the solution conductivity due to its anionic property in water. However, the previous literatures (Bonino et al., 2011; Fang, Liu, Jiang, Nie, & Ma, 2011) demonstrate that the conductivity has nearly no influence on morphology, and the rheological behavior of the solution is the main factor in electrospinning. Therefore, the rheological behaviors of the electrospinning solutions need to be investigated (Fig. 2). The addition of PVA in composite solutions has a significant effect on the shear-thinning behavior of composite solution. Comparing PVA with PVA/OREC solutions as well as PVA/ALG with PVA/ALG/OREC solutions, the zero shear rate viscosity (η) of the solutions decreases strongly when the content of OREC increases. The rheological results demonstrate that the intermolecular interactions are strongly enhanced with the addition of PVA. Furthermore, the enhanced intermolecular interactions are regarded as the key role in improving the electrospinnability of ALG containing solutions (Fang et al., 2011).

3.3. FT-IR spectra

Fig. 3 shows the FT-IR spectra of the bulk powders and composite nanofibrous mats. The frequencies and assignments for the bulk OREC are indicated as follows: 467 and 546 cm^{-1} for Si–O stretching vibration band, 910 and 3643 cm^{-1} for —OH vibration, 1650 cm^{-1} for H_2O bending vibration, 2921 cm^{-1} for —CH_3 group and 2851 cm^{-1} for —CH_2 bending vibration (Guo et al., 2005; Wang et al., 2008). The characteristic peaks of PVA spectra are at 3338 cm^{-1}, which represents the bending vibration of hydroxyl groups. Besides, 2941 cm^{-1} assigns to —CH_2, 1734 cm^{-1} results

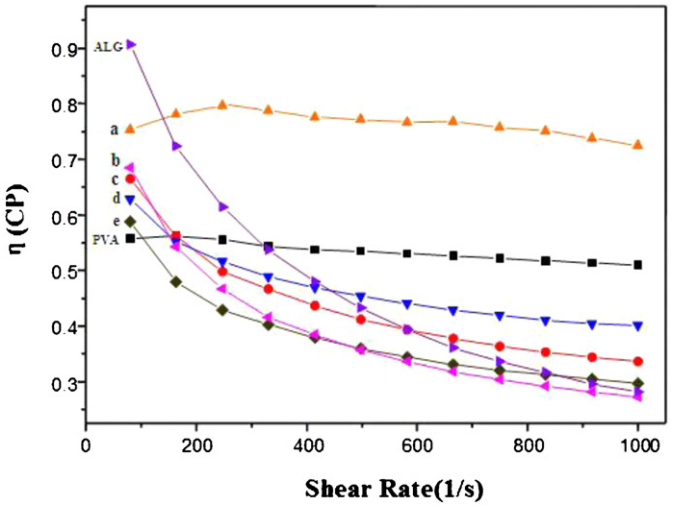

Fig. 2. Rheological behavior of the bulks and composite solutions with various PVA/ALG mass ratios: (a) 100/0 containing 1% OREC, (b) 40/60 containing 1% OREC, (c) 60/40, (d) 80/20 containing 1% OREC and (e) 60/40 containing 1% OREC.

from C=O bending vibration, 1098 cm^{-1} stands for C–O group and 850 cm^{-1} is attributed to C–C group stretching vibration (Deng, Li, & et al., 2011). In the spectrum of ALG, the characteristic peaks of 3430, 615 and 1417 cm^{-1} belong to hydrogen bonded —OH groups, asymmetric —COO— and symmetric —COO— stretching vibrations, respectively (Islam & Karim, 2010). Obviously, the PVA/OREC and PVA/ALG/OREC mats have the Si–O bending vibration at 546 and 467 cm^{-1} which verifies that OREC is in the composite nanofibrous mats (Fig. 3a and c). Moreover, the characteristic peak of OREC at 3643 cm^{-1} disappears when OREC is added into the composite mats. The reason may be that hydrogen bonding is generated between the hydroxyl groups of OREC and PVA or ALG (Deng, Li, & et al., 2011). Compared with PVA spectrum, some characteristic bands around 1417 and 3430 cm^{-1} tend to appear in that of PVA/ALG mats (Fig. 3b) which reveals the interactions exist between PVA and ALG (Islam & Karim, 2010). Obviously, the bands of hydroxyl stretching become more and more widely when ALG is added. The result confirms that —OH of PVA may form ether bond

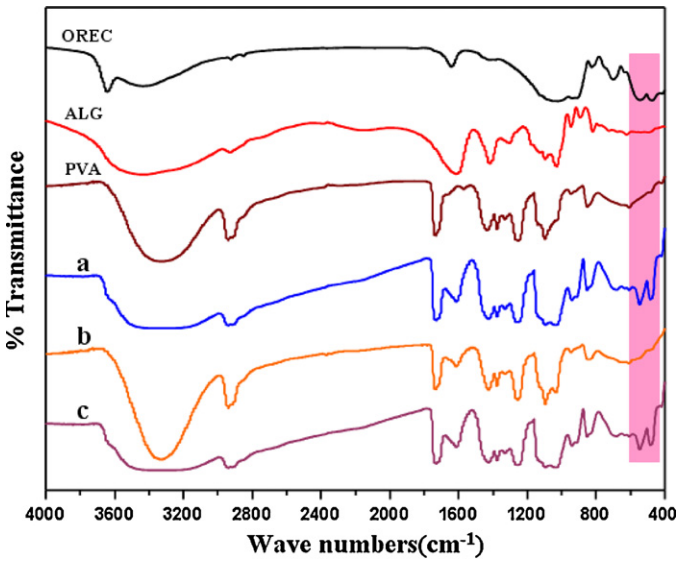

Fig. 3. FT-IR spectra of the bulks and the composite nanofibrous mats with various PVA/ALG mass ratios: (a) 100/0 containing 1% OREC, (b) 60/40 and (c) 40/60 containing 1% OREC.

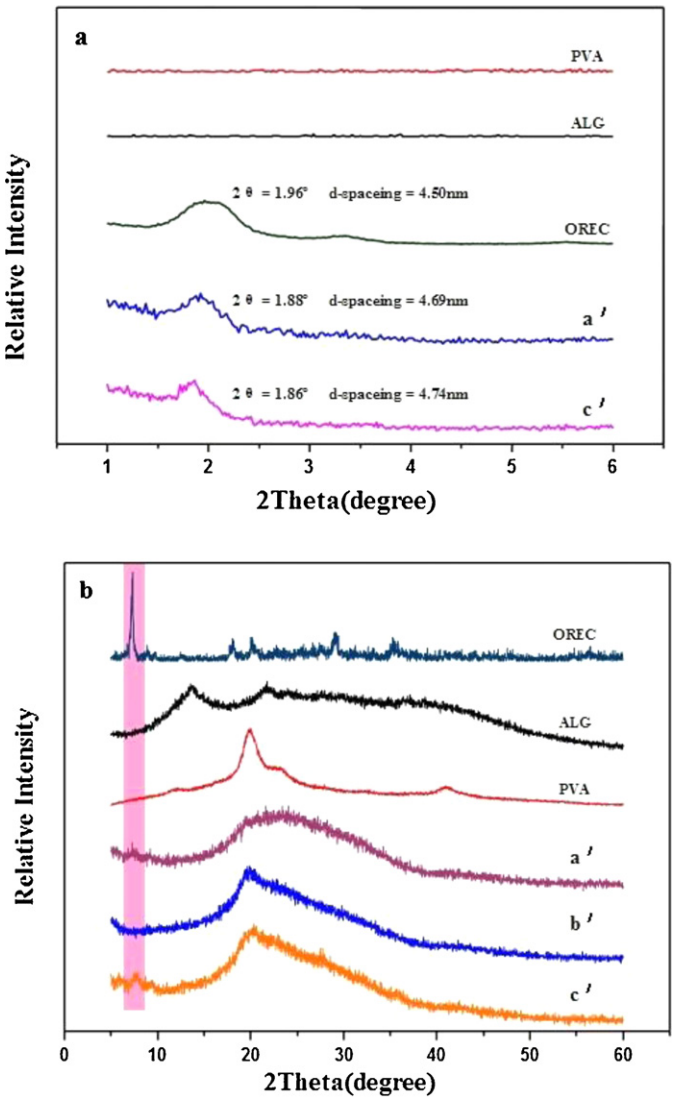

Fig. 4. SAXRD (a) and WAXRD (b) patterns of the bulk and the composite nanofibrous mats with various PVA/ALG mass ratios: (a′) 100/0 containing 1% OREC, (b′) 60/40 and (c′) 40/60 containing 1% OREC.

with the —OH of ALG, and generate hydrogen bonding finally (Islam & Karim, 2010). Furthermore, the interaction between polymers and OREC will be enhanced.

3.4. SAXRD and WAXRD patterns

In order to investigate the building of predesigned intercalated architecture small-angle X-ray diffraction (SAXRD) patterns of bulk materials and nanofibrous mats (Fig. 4a) are analyzed by the change of gallery distance of OREC before and after intercalation. Obviously, both ALG and PVA have no layered structure. According to the SAXRD results, the interlayer distance between OREC is 4.50 nm, which is elucidated by the Bragg's equation. In addition, the spacing distance between OREC interlayers in PVA/OREC nanofibrous mats is enlarged to 4.69 nm. Compare with that of others, the characteristic peaks of PVA/ALG/OREC shifts towards lower angle and the interlayer distance is 4.74 nm. The above results confirm that both PVA and ALG chains are successfully intercalated into the interlayer of OREC.

Fig. 4b presents the wide angle X-ray diffraction (WAXRD) patterns of the bulk and the composite nanofibrous mats. In the WAXRD patterns of OREC, five crystalline peaks at 7.34°, 18.06°, 20°, 29.06° and 35.84° are clearly observed (Wang et al., 2009), and the diffraction of PVA consists of 12.5°, 20°, 23.2° and 40.9°, respectively (Zhang et al., 2007). ALG shows major peaks around 13.5° and 21.6° (Islam & Karim, 2010). Clearly both PVA/OREC and PVA/ALG/OREC nanofibrous mats have the characteristic peak around 7.34° which verifies that OREC is successful incorporated in the composite mats. In addition, a significant peak around 20° in composite nanofibrous mats becomes lower and broader. The reduction of the crystallinity of PVA/ALG nanofibrous mats can be attributed to the hydrogen-bonding interaction between hydroxyl groups in PVA and the hydroxyl or carboxyl groups in ALG (Islam & Karim, 2010). Therefore, the crystalline structure of PVA can hinder the chains of ALG which has a great influence on electrospinnability of the composite solutions. Furthermore, the above results indicate that the strong molecular interactions are contributed by hydrogen bonding between polymers and OREC.

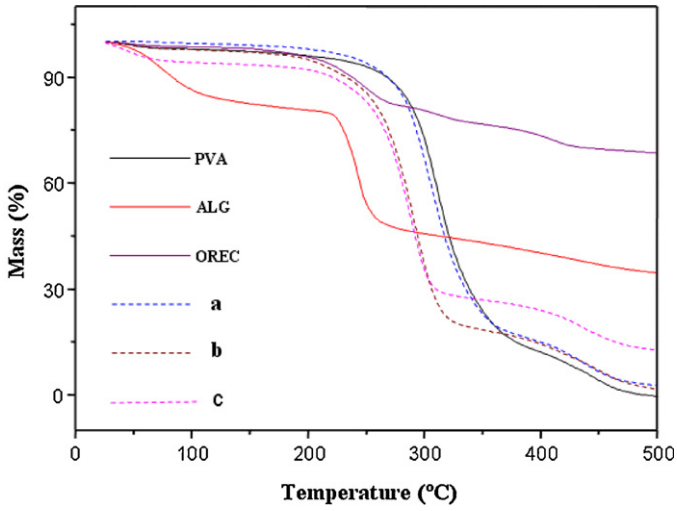

Fig. 5. TGA thermograms of bulks and composite nanofibrous mats with various PVA/ALG mass ratios: (a) 100/0 containing 1% OREC, (b) 60/40 and (c) 40/60 containing 1% OREC.

3.5. Thermal properties

The TGA analysis (Fig. 5) displays the thermal properties of the composite nanofibrous mats. In fact, the structure, molecular weight, and conformation of the polymer play important roles in the depolymerization temperature. PVA chains will form conjugated polyene after the water is removed (Islam & Karim, 2010). Generally, three weight loss peaks are observed in the TGA analysis for bulk PVA (Fig. 5). The first peak between 20 and 100 °C is attributed to water lose, the second peak between 250 and 380 °C is corresponded to the decomposition of PVA, and the third peak between 400 and 500 °C is the carbonization of the degraded products to ash. Indeed, as an inorganic substance, OREC has little mass loss on heating up to nearly 500 °C. Clearly, compared with pure PVA mats, the degradation temperature is improved when ALG is added in composite mats. Besides, the mass loss of mats with OREC is less than that of mats without OREC, which reveals the nanofibrous mats with OREC exhibits better thermal stability. This result demonstrates that the interactions exist between polymers and OREC.

3.6. Antibacterial activity assay

The antibacterial activity assay is measured by disk-diffusion test (Fig. 6). The Gram-negative bacteria *E. coli* and Gram-positive bacteria *S. aureus* are selected as the bacteria for testing the

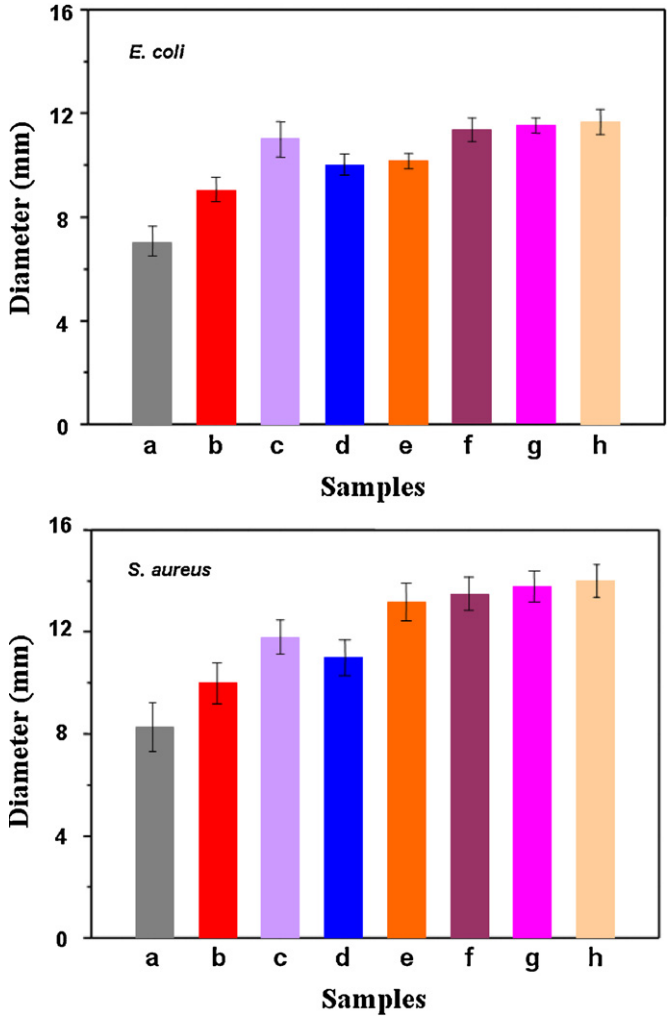

Fig. 6. Antimicrobial activities against *E. coli* and *S. aureus* of: (a) aluminum foil and nanofibrous mats fabricated from various PVA/ALG solutions with different mass ratios: (b) 100/0 and (c) 60/40; and nanofibrous mats electrospun from PVA/ALG solutions at different mass ratios containing 1% OREC: (d) 100/0, (e) 90/10, (f) 80/20, (g) 60/40 and (h) 40/60.

inhibition ability of the composite nanofibrous mats via inhibition zone surrounding circular mats disks. Obviously, no matter what the composite nanofibrous mats are fabricated from, the inhibitory property of the mats against the Gram-positive bacteria are better than that against Gram-negative bacteria (Wang et al., 2006; Deng et al., 2012). As the negative control, aluminum foil disks exhibit a little inhibition ability, and their inhibition zones are around 7 mm against *E. coli* and 8.25 mm against *S. aureus*, respectively. The reason is that when the aluminum foil is covered on the surface of the bacteria colonies (Fig. 6a), the environment where bacteria attached are lacked of O_2 and CO_2, and the bacteria tends to be dead (Deng et al., 2012). Besides, the PVA mats also show a little antibacterial activity (Fig. 6b). Obviously, the degree of bacterial inhibition of nanofibrous mats is remarkably enhanced when the content of ALG is increased. Based on the hydrogel properties, ALG can easily form gel structure which will provide a beneficial physical barrier against bacteria (Walker et al., 2003; Covarrubias et al., 2012). Comparing Fig. 6b with d, the as-spun mats containing OREC has also exhibited enhanced antibacterial activity, which is consistent with the previous reports (Wang et al., 2009; Deng et al., 2012). The increase of bacterial inhibition with the addition of OREC may be caused by three reasons: firstly, the positively charged OREC can absorb the negatively charged bacteria via electrostatic forces, and the bacteria can be immobilized on the surface of OREC. Secondly, OREC exhibits large surface area which also has a great influence on antibacterial activity. Thirdly, the OREC has synergy for enhancing antibacterial activity which can be observed from Fig. 6c and g. To sum up, the association between OREC and bacteria are the main reason why the antibacterial activity of nanofibrous mats is improved (Wang et al., 2009).

4. Conclusions

In this study, PVA/ALG/OREC nanofibrous mats are prepared successfully via electrospinning. The rheological behavior of PVA/ALG/OREC composite solutions plays an important role on the electrospun nanofibrous mats. Besides, the EDX spectroscopy verifies the existence of OREC in the composite mats. In addition, the SAXRD data indicates that the interlayer distance of OREC is increased by the intercalation of polymer chains. The WAXRD and FT-IR results reveal that the hydroxyl group of OREC had intermolecular interaction with the chains of ALG and PVA. Moreover, the thermal stability is considerably improved with the addition of OREC in the composite mats. Furthermore, the antibacterial activity of the as-spun mats is enhanced when the content of OREC is increased. The immobilization of layered silicate into the composite nanofibrous mats with controllable interlayer distance may have great potential values in the application area of food packaging and wound dressing.

Acknowledgments

This project was funded by National Natural Science Foundation of China (No. 31101365) and National Science & Technology Support Program (No. 2012BAD31B10-6), and partially supported by the Fundamental Research Funds for the Central Universities of China (No. 52902-0900202208).

References

Balakrishnan, B., Mohanty, M., Umashankar, P. R., & Jayakrishnan, A. (2005). Evaluation of an in situ forming hydrogel wound dressing based on oxidized alginate and gelatin. *Biomaterials*, *26*, 6335–6342.

Bonino, C. A., Krebs, M. D., Saquing, C. D., Jeong, S. I., Shearer, K. L., Alsberg, E., et al. (2011). Electrospinning alginate-based nanofibers: From blends to crosslinked low molecular weight alginate-only systems. *Carbohydrate Polymers*, *85*, 111–119.

Chen, S. G., Chen, S. J., Jiang, S., Xiong, M. L., Luo, J. X., Tang, J. N., et al. (2011). Environmentally friendly antibacterial cotton textiles finished with siloxane sulfopropylbetaine. *ACS Applied Materials & Interfaces*, *3*, 1154–1162.

Covarrubias, S. A., de-Bashan, L. E., Moreno, M., & Bashan, Y. (2012). Alginate beads provide a beneficial physical barrier against native microorganisms in wastewater treated with immobilized bacteria and microalgae. *Applied Microbiology and Biotechnology*, *93*, 2669–2680.

Deng, H. B., Zhou, X., Wang, X. Y., Zhang, C. Y., Ding, B., Zhang, Q. H., et al. (2010). Layer-by-layer structured polysaccharides film-coated cellulose nanofibrous mats for cell culture. *Carbohydrate Polymers*, *80*, 474–479.

Deng, H. B., Li, X. Y., Ding, B., Du, Y. M., Li, G. X., Yang, J. H., et al. (2011). Fabrication of polymer/layered silicate intercalated nanofibrous mats and their bacterial inhibition activity. *Carbohydrate Polymers*, *83*, 973–978.

Deng, H. B., Wang, X. Y., Liu, P., Ding, B., Du, Y. M., Li, G. X., et al. (2011). Enhanced bacterial inhibition activity of layer-by-layer structured polysaccharide film-coated cellulose nanofibrous mats via addition of layered silicate. *Carbohydrate Polymers*, *83*, 239–245.

Deng, H. B., Lin, P. H., Xin, S. J., Huang, R., Li, W., Du, Y. M., et al. (2012). Quaternized chitosan-layered silicate intercalated composites based nanofibrous mats and their antibacterial activity. *Carbohydrate Polymers*, *89*, 307–313.

Ding, B., Kim, J., Kimura, E., & Shiratori, S. (2004). Layer-by-layer structured films of TiO2 nanoparticles and poly(acrylic acid) on electrospun nanofibres. *Nanotechnology*, *15*, 913–917.

European Food Safety Authority (E.F.S.A). (2011). Scientific opinion on the safety and efficacy of bentonite (dioctahedral montmorillonite) as feed additive for all species. *EFSA Journal*, *9*, 2007–2030.

Fang, D. W., Liu, Y., Jiang, S., Nie, J., & Ma, G. P. (2011). Effect of intermolecular interaction on electrospinning of sodium alginate. *Carbohydrate Polymers*, *85*, 276–279.

Guo, T., Ma, Y. L., Guo, P., & Xu, Z. R. (2005). Antibacterial effects of the Cu(II)-exchanged montmorillonite on *Escherichia coli* K88 and *Salmonella choleraesuis*. *Veterinary Microbiology*, *105*, 113–122.

Hou, Z. Y., Li, C. X., Ma, P. A., Li, G. G., Cheng, Z. Y., Peng, C., et al. (2011). Electrospinning preparation and drug-delivery properties of an up-conversion luminescent porous NaYF4:Yb3+, Er3+@silica fiber nanocomposite. *Advanced Functional Materials*, *21*, 2356–2365.

Islam, M. S., & Karim, M. R. (2010). Fabrication and characterization of poly(vinyl alcohol)/alginate blend nanofibers by electrospinning method. *Colloids and Surfaces a-Physicochemical and Engineering Aspects*, *366*, 135–140.

Lee, J. S., Choi, K. H., Do Ghim, H., Kim, S. S., Chun, D. H., Kim, H. Y., et al. (2004). Role of molecular weight of atactic poly(vinyl alcohol) (PVA) in the structure and properties of PVA nanofabric prepared by electrospinning. *Journal of Applied Polymer Science*, *93*, 1638–1646.

Lee, K. Y., Jeong, L., Kang, Y. O., Lee, S. J., & Park, W. H. (2009). Electrospinning of polysaccharides for regenerative medicine. *Advanced Drug Delivery Reviews*, *61*, 1020–1032.

Li, X. X., Li, X. Y., Ke, B. L., Shi, X. W., & Du, Y. M. (2011). Cooperative performance of chitin whisker and rectorite fillers on chitosan films. *Carbohydrate Polymers*, *85*, 747–752.

Mimura, H., Yan, W., Wang, Y. F., Niibori, Y., Yamagishi, I., Ozawa, M., et al. (2011). Selective separation and recovery of cesium by ammonium tungstophosphate-alginate microcapsules. *Nuclear Engineering and Design*, *241*, 4750–4757.

Noh, H. K., Lee, S. W., Kim, J. M., Oh, J. E., Kim, K. H., Chung, C. P., et al. (2006). Electrospinning of chitin nanofibers: Degradation behavior and cellular response to normal human keratinocytes and fibroblasts. *Biomaterials*, *27*, 3934–3944.

Suci, P. A., Vrany, J. D., & Mittelman, M. W. (1998). Investigation of interactions between antimicrobial agents and bacterial biofilms using attenuated total reflection Fourier transform infrared spectroscopy. *Biomaterials*, *19*, 327–339.

Walker, M., Hobot, J. A., Newman, G. R., & Bowler, P. G. (2003). Scanning electron microscopic examination of bacterial immobilisation in a carboxymethyl cellulose (AQUACEL®) and alginate dressings. *Biomaterials*, *24*, 883–890.

Wang, X. F., Ding, B., Yu, J. Y., & Wang, M. R. (2011). Engineering biomimetic superhydrophobic surfaces of electrospun nanomaterial. *Nanotoday*, *22*, 510–530.

Wang, X. Y., Du, Y. M., Yang, J. H., Tang, Y. F., & Luo, J. W. (2008). Preparation, characterization, and antimicrobial activity of quaternized chitosan/organic montmorillonite nanocomposites. *Journal of Biomedical Materials Research Part A*, *84A*, 384–390.

Wang, X. Y., Du, Y. M., Yang, J. H., Wang, X. H., Shi, X. W., & Hu, Y. (2006). Preparation characterization and antimicrobial activity of chitosan/layered silicate nanocomposites. *Polymer*, *47*, 6738–6744.

Wang, X. Y., Du, Y. M., Luo, J. W., Yang, J. H., Wang, W. P., & Kennedy, J. F. (2009). A novel biopolymer/rectorite nanocomposite with antimicrobial activity. *Carbohydrate Polymers*, *77*, 449–456.

Xu, R., Feng, X., Li, W., Xin, S., Wang, X., Deng, H., et al. (2013). Novel polymer-layered silicate intercalated composite beads for drug delivery. *Journal of Biomaterials Science. Polymer Edition*, *24*, 1–14.

Zhang, Y. Y., Huang, X. B., Duan, B., Wu, L. L., Li, S., & Yuan, X. Y. (2007). Preparation of electrospun chitosan/poly(vinyl alcohol) membranes. *Colloid and Polymer Science*, *285*, 855–863.